Research article

The E3 ubiquitin ligase RBCK1: Implications in the tumor immune microenvironment and antiangiogenic therapy of glioma

Jing Guo [a,b,c,1], Donglin Sun [d,1], Junwei Zhang [a,b,c,1], Jie Guo [a,b,c], Zhenpeng Wu [a,b,c], Yongzhen Chen [e], Yujie Xu [a,b,c], Desheng Zhou [a,b,c], Yachao Cui [a,b,c], Qi Mo [a,b,c], Yingchang Li [a,b,c], Ting Zhao [f,*], Qiang You [a,b,c,e,**]

[a] Affiliated Cancer Hospital & Institute, Guangzhou Medical University, 78 Hengzhigang Road, Guangzhou 510095, China
[b] Key Laboratory of Cell Homeostasis and Cancer Research of Guangdong Higher Education Institutes, Guangzhou Medical University, Guangzhou 510182, China
[c] Center for Cancer and Immunology Research, State Key Laboratory of Respiratory Disease, Guangzhou, China
[d] Department of Urology, Shenzhen Hospital, Southern Medical University, Shenzhen 518100, China
[e] Department of Biotherapy, Second Affiliated Hospital of Nanjing Medical University, Nanjing 210011, China
[f] Department of Medical Oncology, Fudan University Shanghai Cancer Center, Shanghai 200032, China

ABSTRACT

E3 ubiquitin ligases (E3s) play a pivotal role in regulating the specificity of protein ubiquitination, and their significant functions as regulators of immune responses against tumors are attracting considerable interest. RBCK1—an RBR E3 ligase—is involved in immune regulation and tumor development. However, the potential effect of RBCK1 on glioma remains enigmatic. In the present study, we performed comprehensive analyses of multilevel data, which disclosed distribution characteristics of RBCK1 in pan-cancer, especially in glioma. Functional roles of RBCK1 were further confirmed using immunohistochemistry, cell biological assays, and xenograft experiments. Aberrant ascending of RBCK1 in multiple types of cancer was found to remodel the immunosuppressive microenvironment of glioma by regulating immunomodulators, cancer immunity cycles, and immune cell infiltration. Notably, the MES-like/RBCK1[High] cell population, a unique subset of cells in the microenvironment, suppressed T cell-mediated cell killing in glioma. Elevated expression levels of RBCK1 suggested a glioma subtype characterized by immunosuppression and hypo-responsiveness to immunotherapy but manifesting surprisingly increased responses to anti-angiogenic therapy. In conclusion, anti-RBCK1 target therapy might be beneficial for glioma treatment. Moreover, RBCK1 assisted in predicting molecular subtypes of glioma and response rates of patients to different clinical treatments, which could guide personalized therapy.

1. Introduction

Ubiquitination—a reversible post-translational modification—plays a significant role in oncogenesis and immune responses, requiring three enzyme complexes. Among them, E3 ubiquitin ligases (E3s) are the primary regulators of specificity in protein ubiquitination, mainly by recognizing substrates [1,2]. E3s function in various cellular processes, such as DNA repair and metabolism, so dysfunctions of E3s could induce multiple diseases, including cancer. Because of their vital role in cancer immunotherapy, E3s are currently identified as important immune system regulators. Targeting E3s has been considered a promising

treatment to boost antitumor immunity [3].

RANBP2-type and C3HC4-type zinc finger-containing 1 (RBCK1 or HOIL-1L)—a member from the family of the RBR E3 ligases [4,5]—has been found to participate in cell-cycle progression and immune regulation [5–7]. RBCK1 forms the linear ubiquitin chain assembly complex (LUBAC) with HOIP and SHARPIN, responsible for the Met1-linked ubiquitination of substrates related to cell death and immune signaling [8,9]. Remarkably, a genome-scale CRISPR-Cas9 screening study revealed that RBCK1 took part in the resistance building of cancer cells to attack by T cells [10]. Additionally, the deletion of RBCK1 in cancer cells leads to better efficacy of immunotherapy [11,12]. These

---

recent findings indicate that RBCK1 could function as a potential cancer biomarker and therapeutic target. However, its roles in prognosis and immune microenvironment in pan-cancer have not been thoroughly investigated.

The tumor microenvironment (TME) is a complex cellular milieu in which the development and progression of cancer usually involve extensive remodeling [13]. TME is critical in regulating tumor pathogenesis and has a notable effect on influencing therapy responses because tumor-infiltrating immune cells have some crucial functions to play in it [13,14]. Moreover, forming new blood vessels is a critical process in tumor progression. Aberrant vasculatures in TME help neoplasms evade the surveillance and attack of the immune system by establishing an immunosuppressive environment [15]. Therefore, recent studies have sought to investigate the function of RBCK1 in the TME.

Glioma is the most destructive and invasive primary brain tumor, featuring a poor prognosis and limited treatment options [16,17]. Identification of isocitrate dehydrogenase (IDH) mutation, 1p19q codeletion, O6-methylguanine-DNA methyltransferase (MGMT) promoter methylation, and α thalassemia/intellectual disability syndrome X-linked (ATRX) mutation status as prognostic biomarkers have been the major breakthroughs in glioma treatment [18]. Nonetheless, despite advances in therapeutic strategies, the prognosis of glioma remains dismal, with high relapse rates. Unique pro-angiogenic and immune microenvironment differentiates glioma from other solid cancers and leads to great challenges for prognostication and treatment development [19,20]. Therefore, it is urgent to explore relevant biological molecules, which could aid in clinical treatment decision-making and improve clinical outcomes.

The advances in high-throughput sequencing and comprehensive bioinformatics technologies have facilitated the identification of critical regulators and their potential functions in tumor progression. The present study analyzed the expression patterns and immunological functions of RBCK1 in diverse cancer types, especially glioma. Additionally, RBCK1 promoted the formation of suppressive TME, which has the potential to aid in assessing glioma patients' responsiveness to different treatments, which can contribute to tailored therapy design.

2. Materials and methods

Fig. S1 depicts the study's workflow.

2.1. Data processing

The Cancer Genome Atlas Program (TCGA) and Genotype-Tissue Expression (GTEx) project provided unified and standardized data, which were obtained from the UCSC RNA-seq Compendium. Supplementary Table S1 outlines the acronyms for different cancer types. To validate the findings, we obtained RNA-seq and clinicopathological data from the BrainBase database (https://ngdc.cncb.ac.cn/brainbase) and the Chinese Glioma Genome Atlas (CGGA) database. The Gene Expression Omnibus (GEO) database was used to download glioma samples with the scRNA-seq data of GSE131928. Data access policies of each database were honored in this research. RBCK1 protein sequences were gained from UniProt, and its protein domain features are shown in Supplementary Table S2. The structure of RBCK1 was obtained using the AlphaFold prediction. Single-cell RNA sequencing analyses were conducted on four glioma cohorts (GSE102130, GSE148842, GSE89657, and GSE70630) using the Tumor Immune Single-cell Hub (TISCH) [21].

2.2. Analysis of mutation and copy number difference

The UCSC Xena provides the copy number variation (CNV) data, and the package "maftools" was used to acquire and display the mutation data. Based on the GISTIC2 threshold, the copy number status of deletion, normal, and amplification was ascertained [22].

2.3. Tumor mutational burden (TMB), microsatellite instability (MSI), neoantigen (NEO), and stemness Indices

TMB was the total count of somatic mutations, fragment insertions, and deletions per million bases [23]. MSI and NEO data were acquired from prior studies [24,25]. The relevance between RBCK1 expression and TMB, MSI, and stemness indices was examined using Spearman's correlation method.

2.4. Analysis of tumor immune microenvironment characteristics

The ESTIMATE algorithm was used to determine the immune, stromal, and ESTIMATE scores [26]. The abundance of tumor-infiltrating immune cells was evaluated through the CIBERSOR and QUANTISEQ algorithms. Charoentong et al.'s research was used to gather data on major histocompatibility complexes (MHC), cytokines, and receptors [27]. The cancer immunity cycle is a key to anti-cancer immune response, consisting of seven steps, including cancer antigen release, antigen presentation, activation, immune cell transport to the tumor, immune cell infiltration of the tumor, T cell recognition by cancer cells, and cancer cell destruction [28]. Gene data were obtained from the Tracking Tumor Immune Phenotype website, and a single-sample gene set enrichment analysis (ssGSEA) was performed to quantify the activation of these steps. TIDE scores were calculated for glioma patients using the algorithm provided by Jiang et al., which assesses tumor immune dysfunction and exclusion [29].

2.5. scRNA-seq data analysis

The analysis of the *scRNA-seq* data was performed using the "Seurat" R package. Cells with a gene count of less than 200, a detection rate of less than three cells, or a high proportion of mitochondrial genes were removed from the analysis. Dimensionality reduction for visualizing *scRNA-seq* data was performed using the Uniform Manifold Approximation and Projection (UMAP). The "FindAllMarkers" program was used to identify cluster-specific marker genes. For each cell cluster, the cell type was defined according to its marker gene. The CellChat package was used to anticipate the communication among various kinds of cells using *scRNA-seq* [30]. The Monocle3 package was applied to generate cell pseudotime paths (https://cole-trapnell-lab.github.io/monocle3). The DoRothEA package was used to calculate transcription factor (TF) activity [31].

2.6. Identification of differentially expressed RNA

Differential expression gene (DEGs) selection was performed using the "limma" package. The "ClusterProfiler" R package was used for Kyoto Encyclopedia of Genes and Genomes (KEGG) analyses. The Hallmark gene set obtained from MSigDB was used to conduct GSEA. Scores of enrichments for gene features were computed, each representing a well-known cancer-related pathway. Pathway score was computed by adding the levels of positive regulatory members and subtracting the levels of negative regulatory members within any given pathway [32].

2.7. Assessment of the responsiveness of chemotherapeutics and the effectiveness of immunotherapy

The Genomics of Drug Sensitivity in Cancer (GDSC) dataset was used to predict the sensitivity of each sample to various anti-angiogenic agents. A prediction procedure was executed using the "pRRophetic" package. The response of the anti-angiogenic agents was estimated by determining the IC50. We used the online tool Tumor Immune Dysfunction and Exclusion (TIDE) to forecast the effectiveness of immunotherapy at the transcriptome features. A lower TIDE score indicates a better response to immunotherapy.

2.7.1. Identification of candidate small molecules

We obtained data on certain genes-associated molecules and chemotherapeutic drug sensitivity from the GSCALite ground on the GDSC. The Connectivity Map (CMAP) database was used to search for possible drugs based on a particular gene expression pattern [33]. The list of potential agents and their scores was obtained by feeding the DEGs into CMAP. Drugs with negative scores have the potential capability to counteract desired biological features and could be therapeutically valuable. All drugs with a score below −95.0 were assessed.

2.8. Cell culture

Human glioma cells and human umbilical vein endothelial cells (HUVECs) were obtained from Wuhan Pu-Nuo-Sai Life Technology Co. Ltd. (Wuhan, China) and the Chinese Academy of Sciences, respectively. Glioma cells were cultured in Dulbecco's modified Eagle medium (DMEM) containing 10% fetal bovine serum (FBS), whereas RPMI 1640 medium containing 10% FBS was used to sustain HUVECs. These cells were placed in a 5% CO_2 incubator and incubated at 37 °C.

2.9. Cell transfection

RBCK1 knockdown short hairpin RNA (shRNA) lentiviral plasmid was conducted by Tsingke Biotechnology Co., Ltd. (Beijing, China). Glioma cells (U87MG and A172) were transfected with these lentiviruses with Lipofectamine 3000 (Thermo Fisher Scientific, Inc.) following the manufacturer's guidelines. Following shRNA-targeting sequences of RBCK1 were used: shRNA-1, CCACAACACTCATCTGTCAAA; shRNA-2, CCCTGAGGATTACCAGCGATT.

2.10. Tumor conditioned medium

The cells were cultured in six-well plates, and then the normal medium was substituted with a serum-free medium. After a day, the supernatant was harvested, centrifuged at 200g for 10 min, and filtered through 0.22-µm syringe filters to obtain tumor-conditioned medium (TCM). The TCM was used for conducting migration and apoptosis assays of HUVECs.

2.11. Western blot analysis

To lyse cells, we used RIPA buffer with protease and phosphatase inhibitors (Beyotime, Shanghai, China). Protein content was quantified using the BCA assay, and the samples were separated in 10% SDS-PAGE gels. The proteins were moved onto a PVDF transfer membrane and later blocked with a blocking solution. After that, primary antibodies were incubated on the membrane at 4 °C overnight, followed by HRP-conjugated secondary antibodies. A chemiluminescence kit was used for protein visualization.

2.12. Real-time quantitative PCR assay

Total RNA was isolated with the TRIzol reagent (Invitrogen, USA) and reversely transcribed. Following primer pairs were used for the RT-qPCR assays: 5'-GAGGGCAGAATCATC ACG AAG-3' and 5'-TGTGCT GTAGGAAGCTCATCTCTC-3' for human VEGFA; 5'-CGTCAC-CAACTGGGACGA- and 5'-ATGGGGGAGGGCATACC-3' for human β-ACTIN.

2.13. Wound healing assay

HUVECs were seeded in six-well plates and allowed to reach complete confluency. Subsequently, the supernatant was discarded, and TCM was added. Wound closure was observed and assessed under a microscope after 48 h.

2.14. Flow cytometry

HUVECs were seeded into 6-well plates and incubated with a tumor-conditioned medium for 48 h. The cells were dissociated using trypsin and resuspended. After washing with PBS, the cells were suspended in a binding buffer. The cells were then exposed to Annexin V-APC and PI and analyzed using flow cytometry. Cell apoptosis was assessed using FlowJo software (FlowJo, LLC, Bethesda, USA).

2.15. Luciferase reporter assays

HIF-1α activity was measured using the hypoxia response element-dependent (HRE-dependent) luciferase assay via the Dual-Luciferase reporter assay system (Promega, Madison, WI). The HIF-1α-responsive luciferase construct containing hypoxia response elements fused with a firefly luciferase was obtained from Addgene (HRE-luciferase, plasmid cat #26731).

2.16. Cell proliferation assay

HUVECs were seeded at 5×10^3 cells/mL in a 96-well plate and incubated with a combination of TCM and Axitinib (0.1 µM) at 37 °C. CCK-8 solution was added after 72 h, and the cells were incubated at 37 °C for 3 h. Absorbance was measured at 450 nm.

2.17. Clinical tissue samples, Hematoxylin and Eosin (HE) staining, and immunohistochemistry (IHC) assay

The Hospital Ethics Committee of the Affiliated Cancer Hospital and Institute of Guangzhou Medical University granted approval for using patient samples following the Declaration of Helsinki. For HE staining, tissue was fixed, paraffin-embedded, dewaxed, rehydrated, and then stained with HE for histopathological analysis. Tissue sections were subjected to deparaffinization, rehydration, and antigen retrieval before undergoing IHC. Following blocking solution incubation, sections underwent overnight incubation with the primary antibody at 4 °C, then treated with biotinylated secondary antibody and HRP-polymer at 37 °C for 30 min

2.17.1. Xenograft experiments

BALB/c nude mice aged 4–5 weeks were housed under stable conditions of 25 °C and a 12-h light-dark cycle. The animal studies were authorized by the Guangzhou Medical University Biomedical Research Ethics Committee and were conducted according to the Guide for the Care and Use of Laboratory Animals. The mice were arbitrarily divided into two groups of six mice each. To establish U87 xenografts, we injected mice subcutaneously with 1×10^6 U87 cells stably transfected with sh-RBCK1 or sh-NC. Tumor formation was monitored for approximately 3 weeks, and tumor sizes were measured every 5 days. Upon completion of the processes, the mice were sacrificed, and tumors were harvested and weighed to calculate tumor volume.

2.18. Statistical analysis

To assess the relationships between variables, we applied Pearson and Spearman correlation coefficients, whereas pairwise comparisons were conducted with either Student's t-test or Wilcoxon rank-sum test. One-way analysis of variance (ANOVA) and the Kruskal-Wallis test were used to compare more than two groups. Kaplan-Meier estimator was used to create survival curves for prognostic evaluations of categorical variables. The R software (version 4.1.2) was used to perform bioinformatics analysis. Statistical differences for cell experiments were determined using GraphPad Prism 8 software. Values are presented as mean ± standard error of means. $P < 0.05$ was deemed statistically significant.

3. Results

3.1. Pan-cancer expression pattern and prognostic significance correlation of RBCK1

RBCK1 possesses an N-terminal LUBAC-tethering motif (LTM), a Ubiquitin-like (UBL) domain, a RanBP2 (NZF) domain, and a canonical RING1 domain is followed by two zinc-coordinating domains known as IBR (In-between-RING) and RING2 (Fig. 1A-B). RING1, IBR, and RING2 are components of the RBR domain, which are essential for the efficient functioning of RBCK1. LTM-mediated RBCK1/SHARPIN interaction plays a critical role in trimeric LUBAC stabilization and function.

Compared with corresponding normal tissues, upregulation of RBCK1 was observed in multiple cancer types, such as glioma (GBMLGG) and breast invasive carcinoma (BRCA) (Fig. 1C). RBCK1 was detected in multiple tumor cell lines, including glioma cells, upon examining the gene expression data of The Human Protein Atlas (Fig. S2A).

Based on the aforementioned results, we then analyzed the potential prognostic relevance of RBCK1 in diverse types of cancer. Despite its varying prognostic value, increased expression of RBCK1 was linked to unfavorable prognosis among several cancer types (Fig. 1D). Similarly, ascended level of RBCK1 led to poorer progression-free survival (PFS) and disease-free survival (DFS) in various cancers, including glioma (Figs. S2B-C).

The K-M plotter was used to plot survival curves based on RBCK1 expression in the TCGA glioma cohort (Fig. 1E-F, S2D). The expression of RBCK1 was positively correlated with the World Health Organization (WHO) grades of glioma (Fig. 1G). Furthermore, a significant upregulation of RBCK1 was observed among patients with IDH-wildtype (Fig. 1H). By contrast, the expression of RBCK1 was elevated in the 1p/19q codeletion group compared with the non-deletion group (Fig. 1I) and did not exhibit an association with MGMT mutation status (Fig. 1J). Moreover, based on the CGGA microarray datasets, the expression of RBCK1 was found to be positively linked to survival rates, WHO grades, and histological type of the glioma and enhanced in the IDH-wildtype and 1p/19q non-deletion groups (Figs. S2E-H). RBCK1 expression showed significant relevance with tumor malignancy and patient prognosis, particularly in cases of glioma.

3.2. Mutational analyses of RBCK1 in pan-cancer

First, we identified the primary somatic mutation signature associated with TCGA glioma patients. Missense mutations were the most common mutation type, single nucleotide polymorphism (SNP) had the highest frequency of variations, and C > T was the predominant mutation type detected in TCGA glioma patients (Figs. S3A-E). The leading 10 genes with mutations in the TCGC glioma cohort are shown in Fig. S3F.

An analysis of different CNV states (neutral, loss, and gain) and mRNA expression data was performed, revealing significant differences in RBCK1 expression among CNV state subgroups in various cancers (Fig. 2A). Further, significant differences in the CNV score of RBCK1 were observed among glioma WHO grades, IDH-status, 1p19q codeletion status, and MGMT promoter methylation status (Fig. 2B-E). Types and locations of RBCK1 somatic mutation rates are presented in Fig. 2F, and the missense mutation mainly in the IBR-type zinc finger domain is an amino acid change at position 352 (p.Arg 352 Gln) from the TCGA glioma cohorts (Fig. S3G). This sequence change replaces the basic and polar arginine with the neutral and polar glutamine. Research has demonstrated that the UbcH7(C86K)-Ub conjugate binds to the RBCK1 RBR-helix in the presence of the allosteric activator M1 di-Ub. Furthermore, within the RBR module of RBCK1, there exists an allosteric ubiquitin (Ub) binding site at the RING1-IBR interface. Notably, RBCK1 I358, in close proximity to the R352Q mutation site, plays a central role in this allosteric Ub binding site. Compared with the wild-type RBCK1, the RBCK1 I358R mutant exhibits weaker activation by M1-linked di-Ub. Additionally, the linked di-Ub fails to bind to RBCK1 I358R [34]. In the protein structure of the RBCK1/UbcH7-Ub/Ub complex (PDB: 8EAZ) [34], R352 and I358 reside on the same helix. However, their side chains are oriented in opposite directions (Fig. S3H). Unlike I358, R352 does not reside on the interaction surface with the allosteric Ub. Notably, the side chain of R352 in RBCK1 is close to D32 of Ub in UbcH7-Ub (Fig. S3H). Therefore, the side chain of RBCK1 R352 has the potential to form hydrogen bonds and/or ionic bonds with the main chain C=O and the side chain of Ub D32, despite the weak electron density of RBCK1 R352 in the RBCK1/UbcH7-Ub/Ub complex. The interaction between RBCK1 R352 and Ub D32 may not be strong. These interactions may enhance the affinity between RBCK1 and UbcH7-Ub. Consequently, when the IBR domain of RBCK1 undergoes a point mutation at R352Q, there is a possibility that this alteration could influence the binding properties of the site. As a result, this mutation has the potential to weaken the binding between RBCK1 and UbcH7-Ub.

As shown in Fig. 2G, the frequencies of the top 15 frequently mutated genes in the RBCK1-high group differed from those in the RBCK1-low group.

3.3. Pan-cancer genomic heterogeneity, immunomodulators, and immune cell infiltration correlation of RBCK1

MSI is a type of genomic instability caused by the deficiency of mismatch repair [35]. TMB is used to quantify non-synonymous somatic mutations occurred in genomic coding regions [36]. These two factors are considered not only involved in tumorigenesis but also as candidates to predict immunotherapeutic responsiveness [35,37,38]. Here, we found that the expression of RBCK1 exhibited varying degrees of significant correlation with TMB, MSI, neoantigen, and stemness across different types of cancers (Fig. 3A-B, S4A-B). Notably, RBCK1 was positively correlated with TMB and stemness indices in glioma. However, the positive association between RBCK1 and neoantigen failed to achieve statistical significance. Similarly, the negative association between RBCK1 and MSI was not statistically significant.

Immune checkpoint genes are crucial for immune cell infiltration, which can influence the effectiveness of immunotherapy [39]. Therefore, a pan-cancer analysis of immune-related effects of RBCK1 was performed to identify patients who could potentially benefit from RBCK1-targeted therapy. We found that RBCK1 expression was positively correlated with LAG3, an immune suppressor gene, in glioma. However, there was a statistically nonsignificant positive relation between RBCK1 and PD-1 (PDCD1), CTLA4, and PD-L1 (CD274) (Fig. 3C). Besides, no significant association was observed between RBCK1 and immune stimulator genes, except for TNFRSF4 and CD40 (Fig. S4C).

Various chemokines have been deemed to modulate tumor immunity [14]. The expression levels of RBCK1 were positively associated with most chemokines and receptors in multiple cancers but inversely correlated with CX3CL1/CX3CR1 in glioma (Fig. S5A), the up-regulation of which would result in the activation and infiltration of immune effector cells in TME [40]. Moreover, RBCK1 was observed to be positively associated with HLA-G, a kind of MHC-I molecule that cancer cells use to engineer a key immune escape mechanism (Fig. S5A) [41].

We then estimated the correlation of RBCK1 with infiltration scores of tumor stroma and immune cells (Supplementary Table S3, Fig. S5B). In glioma, RBCK1 expression positively correlated with immune score and ESTIMATE score but not stromal score. High RBCK1 expression was related to elevated infiltration levels of regulatory T cells (Tregs), M2 macrophages, and neutrophil cells in glioma (Fig. 3D). An additional QUANTISEQ algorithm analysis revealed a positive association between RBCK1 and M2 macrophage infiltration (Fig. S5C). Nevertheless, RBCK1 was found to be negatively correlated with certain effector genes of CD8 + T cells, T helper type 1 (Th1) cells, natural killer (NK) cells, dendritic cells (DC) cells, and macrophages (Fig. 3E).

The chemokine system and other immunomodulators could directly
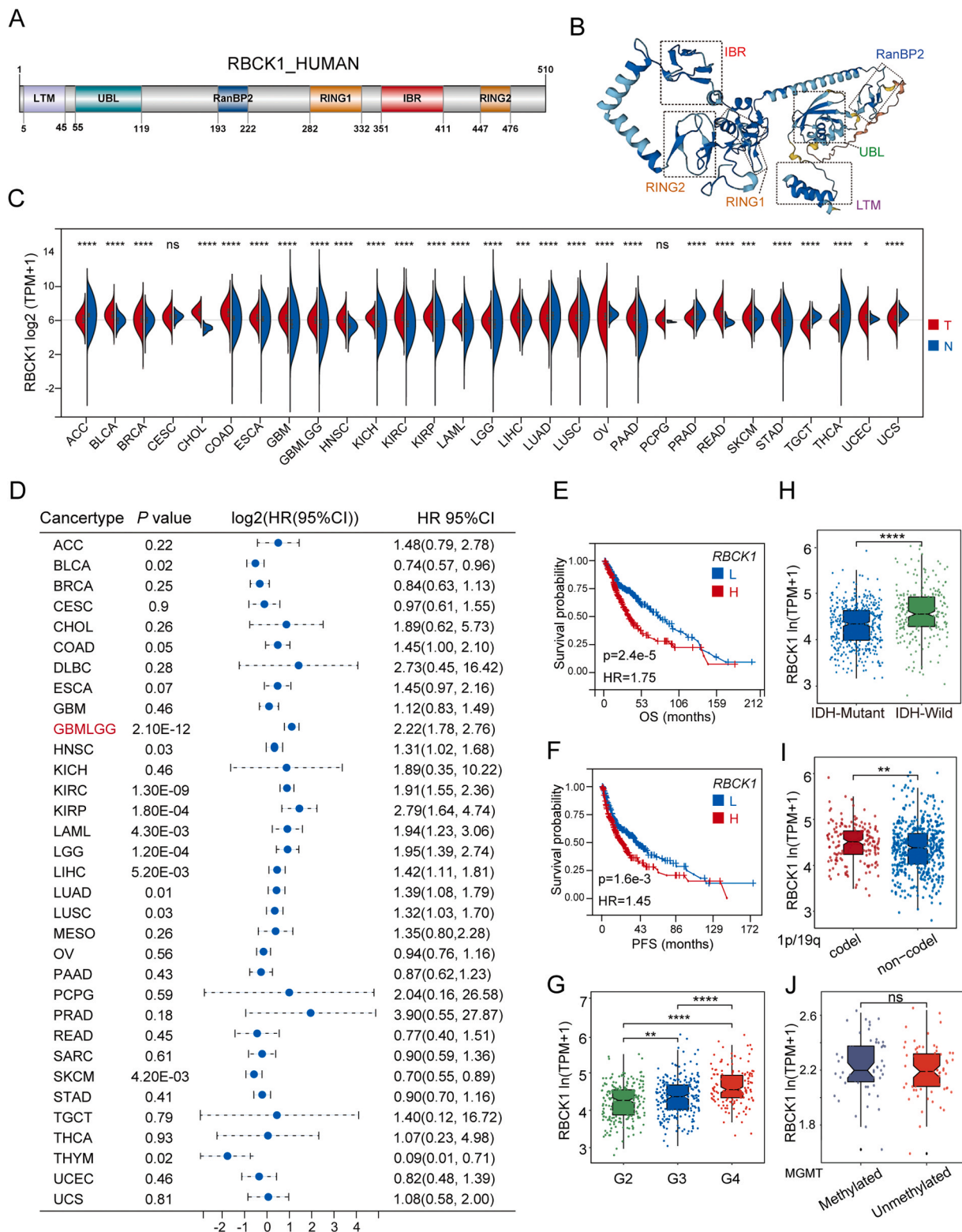
Fig. 1. RBCK1 expression levels in pan-cancer. (A) Schematic diagram of the domains of the RBCK1 protein. (B) Three-dimensional structure of RBCK1 protein from AlphaFold. AlphaFold produced a per-residue confidence score (pLDDT) between 0 and 100. Blue: Very high (pLDDT > 90), cyan: Confident (90 > pLDDT > 70), gold: Low (70 > pLDDT > 50), coral: Very low (pLDDT < 50). (C) RBCK1 expression levels in pan-cancer tissues and corresponding normal tissue (t-test). T, tumor tissue; N, normal tissue; TPM: transcript per million. (D) Correlation between RBCK1 expression levels in OS of pan-cancer. HR, hazards ratio; CI, confidence interval. (E-F) The OS (E) and PFS (F) curves in the TCGA glioma cohort. L, low RBCK1 expression; H, high RBCK1 expression; OS, overall survival; PFS, progression-free survival. (G-J) Expression analysis of RBCK1 in different WHO grades (G2–4, grade2–4) (G), IDH mutant-type and IDH wild-type (H), 1p/19q_codel and non-codel (I), MGMT Methylated and Unmethylated (J) of TCGA glioma cohort using the Brainbase database. Data were analyzed using a t-test for two groups and ANOVA with multiple comparisons. ****$P < 0.0001$, ***$P < 0.001$, **$P < 0.01$, *$P < 0.05$, ns $P > 0.05$.
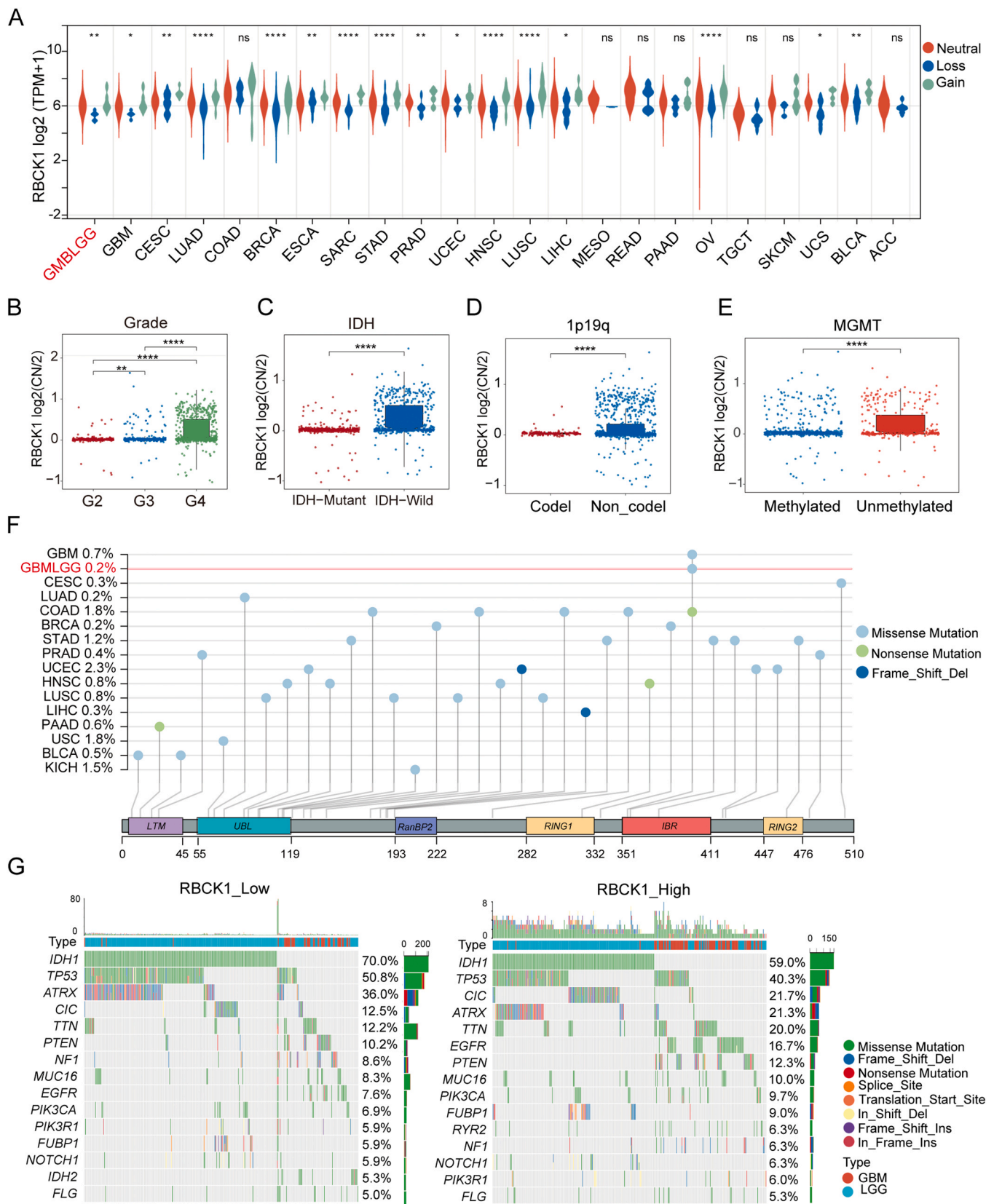
Fig. 2. The mutation and CNV of RBCK1 in pan-cancer. (A) The relationship between different CNV patterns and mRNA expression levels of RBCK1. RBCK1 log2(CN/2) was used to represent RBCK1 copy number variation. CN, copy number. (B-E) The CNV of RBCK1 in different WHO grade(B), IDH mutant and wild-type(C), 1p19q_nodel and non_codel (D), MGMT Methylated and Unmethylated (E) of glioma in the TCGA glioma cohort (G2–4, grade2–4). (F) Mutational landscape of RBCK1 across pan-cancer. The numbers next to the cancer types indicate the mutation frequency of RBCK1. (G) Waterfall of the top 15 mutated genes of glioma patients in the low- and high-RBCK1 groups. Data were analyzed using a t-test for two groups and the Kruskal-Wallis test with multiple comparisons. ***$P < 0.001$, **$P < 0.01$, *$P < 0.05$, ns $P > 0.05$.
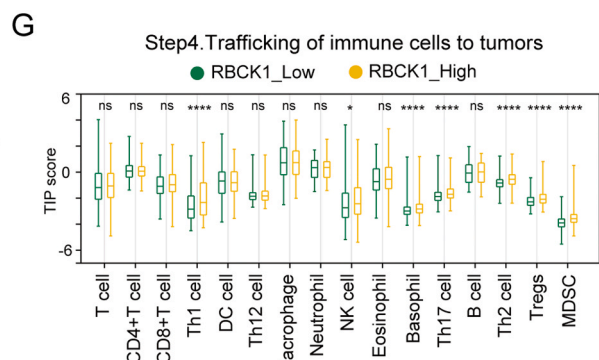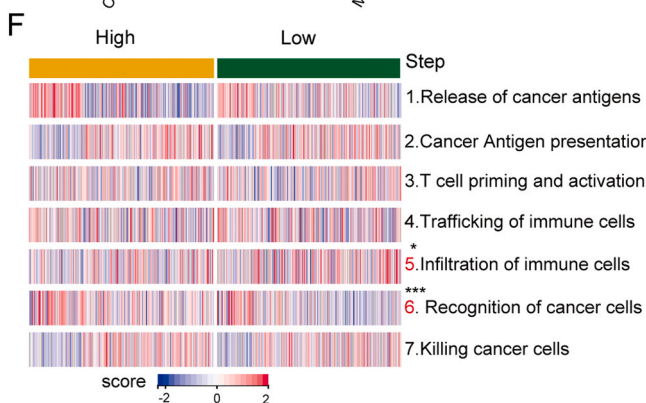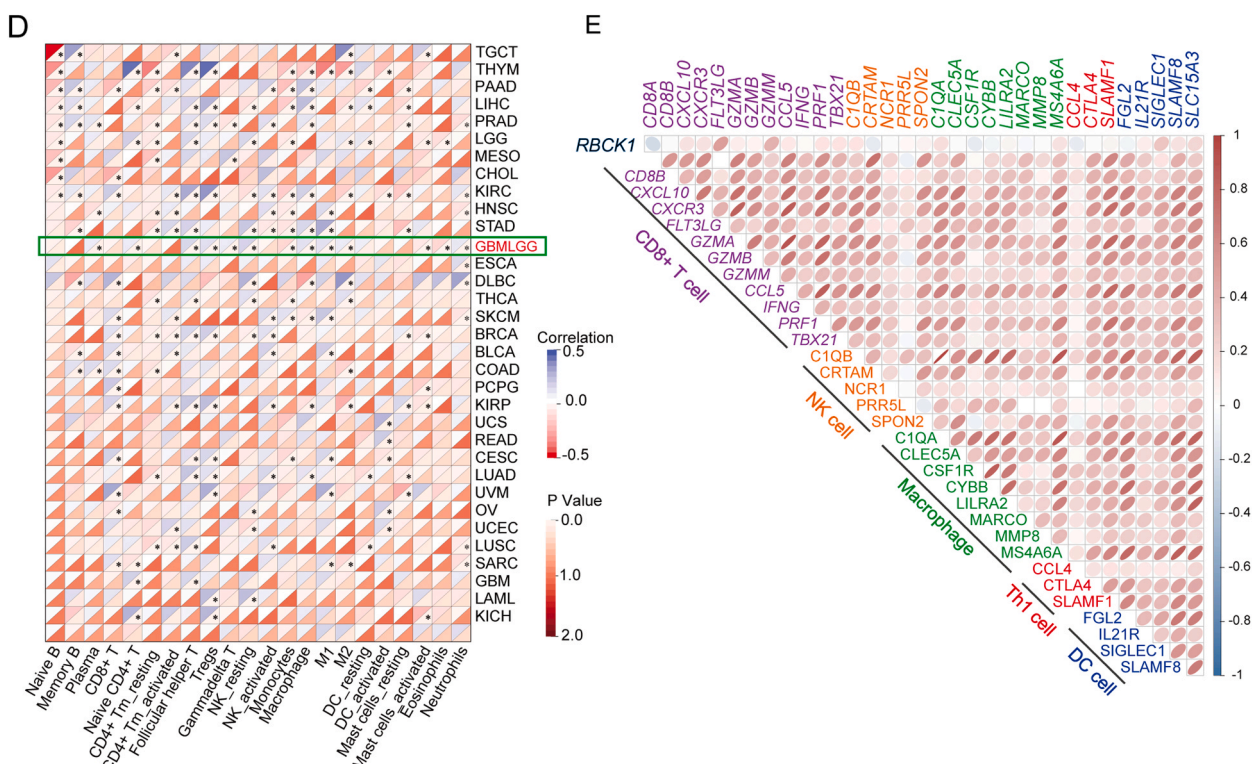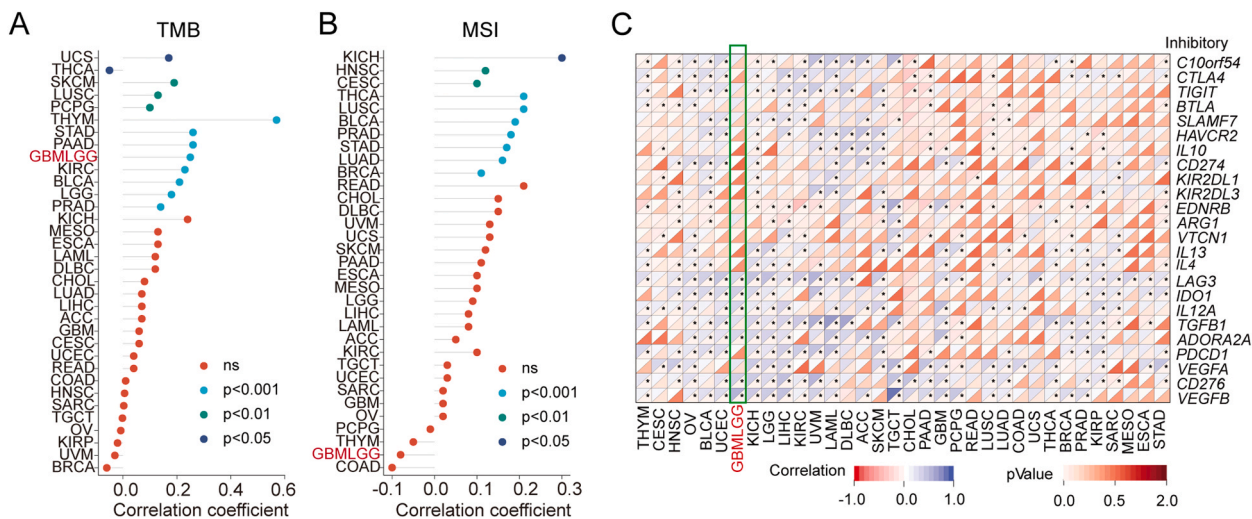
(caption on next page)

Fig. 3. The effect of RBCK1 on immunological status in pan-cancer. (A-B) Relations between RBCK1 expression and TMB (A) and MSI (B) in pan-cancer (Spearman's correlation coefficient). (C) Heatmap of the correlation between RBCK1 and inhibitory immune checkpoints in pan-cancer. (D) Correlation of RBCK1 expression with immune cell infiltrates based on the CIBERSORT algorithm in pan-cancer. The asterisks indicate statistical significance ($P < 0.05$). (E) Correlations between RBCK1 and the effector genes of five immune cells (Pearson correlation analysis). A stronger correlation is indicated by a thinner ellipse, and a weaker correlation by a rounder oval. Negative correlations are represented by blue, and positive ones by red. (F) The thermogram shows the status of anti-cancer immunity steps among the low- and high-RBCK1 groups. (G) Comparison of the proportion of tumor-infiltrating immune cells (Step 4) between low- and high-RBCK1 group (Wilcoxon test). Tm, Memory T cells; Tregs, T regulatory cells; NK, natural killer cell; M1, M1_like macrophages; M2, M2_like macrophages; DC, dendritic cell; Th, helper T cell; MDSC, Myeloid-derived suppressor cell. ****$P < 0.0001$, ***$P < 0.001$, *$P < 0.05$, ns $P > 0.05$.

influence the activities of different parts of the cancer immunity cycle [28]. Infiltration of immune cells into tumors (Step 5) was observed to be downregulated in the high-RBCK1 group. By contrast, the activity of T cell recognition of cancer cells (Step 6) was downregulated in the low-RBCK1 group (Fig. 3F). The differences in immune cell trafficking among Step 4 were further investigated (Fig. 3G). We observed ascended infiltration levels of immunosuppressive cells in the high-RBCK1 group, including T regulatory cells (Tregs), Myeloid-derived suppressor cells (MDSCs), and Th2 cells. Overall, we speculate that RBCK1 regulates remodeling of the TME in glioma, shifting it from an immune-active to an immune-suppressive state.

3.4. The single-cell localization analysis of RBCK1 in the TME of glioma

Besides TME, tumor heterogeneity is an important factor influencing drug response and prognosis. We used four scRNA-seq databases to examine whether RBCK1 expression varies in different subpopulations of malignant cells upon a single-cell level (Figs. S6A-D). Glioma cells were subdivided into four dynamic cell conditions: mesenchymal-like (MES-like), neural-progenitor-like (NPC-like), oligodendrocyte-progenitor-like (OPC-like), and astrocyte-like (AC-like) states [42]. MES-like glioma cells could facilitate the transition of macrophages to a mesenchymal program state and are susceptible to T-cell-mediated killing [43]. Furthermore, UMAP dimensionality reduction was used to visualize the distribution and dissimilarity of different cell types (Fig. S7A), and the top differentially expressed genes from each pooled population were identified (Fig. S7B). Using cluster-specific markers to label different cell types, we divided MES-like cells into two groups based on RBCK1 expression. We used cluster-specific markers to label cell types (Fig. 4A), and MES-like/RBCK1^{High} cells were shown to express high-level RBCK1 in the expression profile (Fig. 4B).

To investigate the interaction among different cell types, we performed analyses with CellChat, in which MES-like/RBCK1^{Low} cells were suggested to have stronger interactions with other cells than MES-like/RBCK1^{High} cells, both in number and probabilities of interactions (Fig. 4C, S7C). We defined two outgoing and four incoming patterns (Fig. 4D, S7D). Particularly, MES-like/RBCK1^{High} in outgoing pattern2 was found to be associated with the secretion of MIF, PTN, MK, PSAP, VISFATIN, ANGPTL (Angiopoietin-like), PARs, FGF, IL16, and PDGF. The main ligand-receptor interactions were also identified (Fig. S7E). Besides, paracrine signaling of COMPLEMENT from MES-like cells to non-MES-like cells was observed mainly to be produced by MES-like/RBCK1^{Low} cells and target monocytes and macrophages (Fig. 4E), which was in line with the findings by Hara T et al. [43], suggesting that MES-like/RBCK1^{Low} cells may affect the pro-inflammatory status of macrophages and exhibit a greater sensitivity to T-cell-mediated killing. PDGFC and PDGFRA, the major players of PDGF singling, were highly expressed in MES-like/RBCK1^{High} cells, whereas MES-like/RBCK1^{Low} cells had high expression of C3, which has a significant effect on the activation of the COMPLEMENT signaling (Fig. 4F).

Pseudotime trajectory analysis was performed on subpopulations of MES-like cells, in which the development of MES-like/RBCK1^{Low} cells in clusters 13 and 9 preceded MES-like/RBCK1^{High} cells in clusters 0, 6, 7, and 10, based on their temporal sequence in cell developmental trajectory (Fig. 4G-H). On account of differentially expressed genes in MES-like/RBCK1^{High}, we performed a KEGG analysis, which revealed that upregulated genes were associated with VEGF, HIF-1, PD-L1 expression,

and PD-1 checkpoint, PI3K-Akt signaling, and tumor transcriptional misregulation (Fig. 4I). Further analyses of transcription factor activities suggested that MES-like/RBCK1^{High} cluster exhibited higher activity of transcription factors SOX10. By contrast, the activity of SMAD3 was increased in the MES-like/RBCK1^{Low} cluster (Fig. 4J). Therefore, RBCK1 might affect the differentiation state of the glioma cells of origin and alter the phenotypes of the subsequent tumors and antitumor immunity.

3.5. Differentially expressed genes and Functional enrichment analysis

Differentially expressed genes in RBCK1-high and RBCK1-low groups were further screened for identifying the molecular function RBCK1 (Fig. S8A). Subsequent gene ontology (GO) analysis of DEGs was enriched in pathways related to NF-κB activity, blood vessel morphogenesis, cell migration, and T cell differentiation (Fig. S8B). Additionally, GSEA analysis revealed that the Hedgehog pathway was significantly activated in the RBCK1-low group, whereas angiogenesis and the TNF-α/NF-κB/Snail pathway were activated in the RBCK1-high group (Figs. S8C-D).

Glioma is deemed a highly malignant solid tumor because of its strong invasiveness and resistance to treatment. Dynamic imaging studies have demonstrated that glioma cells frequently migrate through tissue via blood vessels [44]. Notably, the DEG analysis between the high and low RBCK1 groups identified 48 angiogenesis-related genes, 36 exhibiting increased expression in the high-RBCK1 group (Fig. S8E).

Next, we performed an analysis containing nine anti-angiogenic agents to predict the IC50 values in different groups. The IC50 values of four drugs (Axitinib, Masitinib, Pazopanib, and Sorafenib) were found to be lower in the RBCK1-high group (Fig. 5A), indicating that RBCK1 expression was associated with sensitivity of patients to these drugs. We also found that the expression of endothelial cell-specific genes, including CLEC14A, PECAM1, CDH5, and CLDN5, were positively correlated with RBCK1 (Fig. 5B-E). These findings suggest that RBCK1 assists in vascularizing glioma, making tumor cells more susceptible to anti-angiogenic therapy.

3.6. Predictive value of RBCK1 on immunotherapeutic and anti-angiogenic therapy responses in glioma

Given the characteristics of RBCK1 in building vascular microenvironment, glioma patients with elevated levels of RBCK1 were assumed to be responsive to anti-angiogenic treatment. Published bulk RNA-seq data from the REGOMA trial, which evaluated the efficacy of an anti-angiogenic agent termed regorafenib [45,46], was used to perform analyses in which patients exhibiting high levels of RBCK1 expression displayed an increased responsiveness to anti-angiogenic therapies (Fig. 6A-B).

Next, we analyzed a data set of PD-1-inhibitor-treated glioblastoma [47]. We did not observe significant correlations between the expression of RBCK1 and PFS or OS before accepting PD-1 inhibitor therapy; poor PFS and OS after receiving PD-1 inhibitor treatment were related to high expression of RBCK1 (Fig. 6C-D). However, statistical significance was not achieved in the cases, possibly due to the limited number of samples and the high variability within the group. We also noted that in the post-treatment cohort, but not in the pre-treatment cohort, RBCK1 expression was negatively correlated with cytotoxic T cells (Fig. 6C-D), which may be caused by T cells selectively targeting
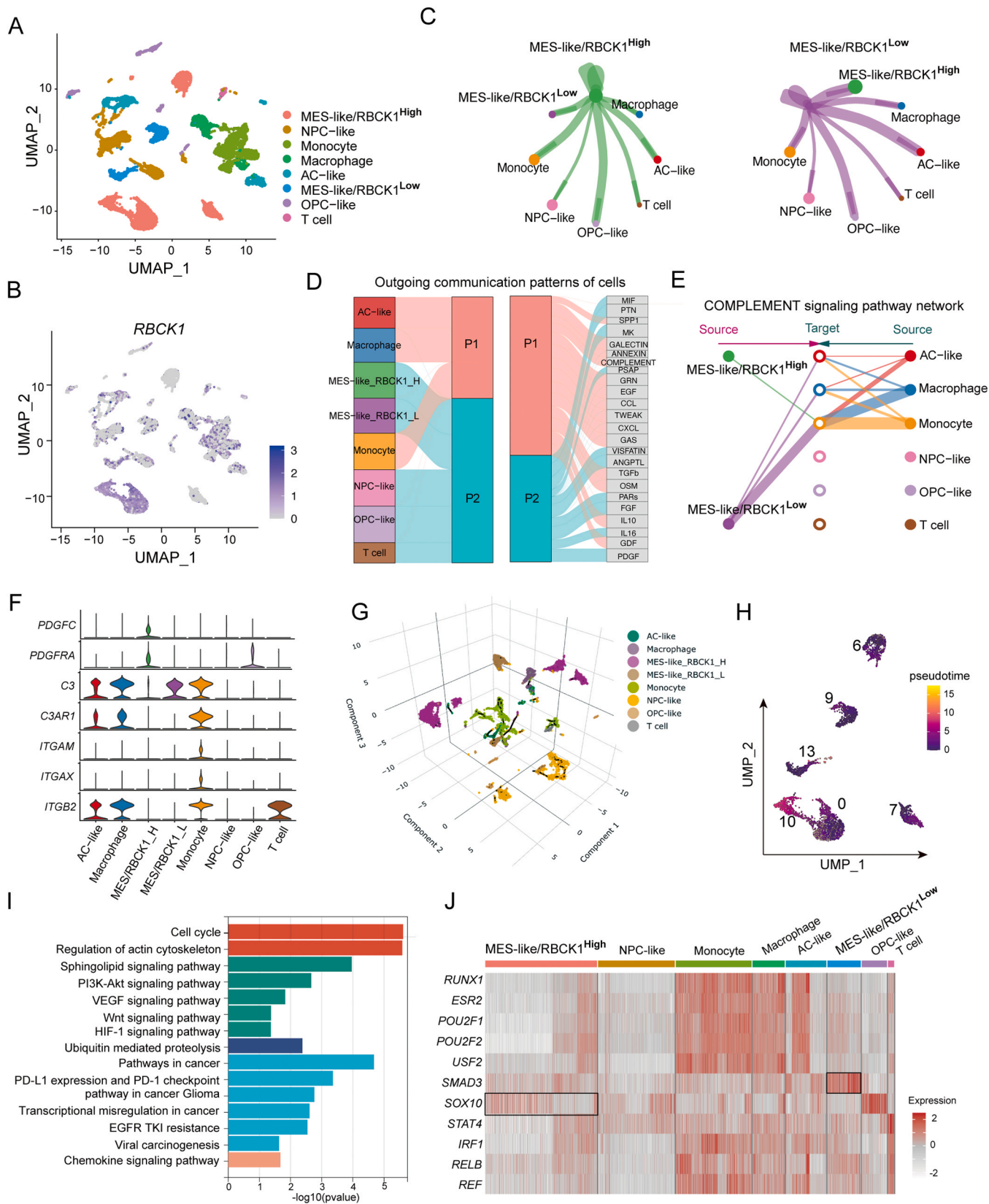
(caption on next page)

Fig. 4. RBCK1 expression in single-cell transcriptome analysis of glioma. (A) UMAP was used to visualize the distribution and dissimilarity of cell types in scRNA-seq data (GSE131928) (B) UMAP plot showing expression of RBCK1. (C) Interactions between the different cell types were analyzed using CellChat with cells from MES-like/RBCK1^{High} (left) and MES-like/RBCK1^{Low} (right). The line thickness indicates the number of ligand-receptor pairs for each interaction. (D) The alluvial plot visualizes the outgoing signaling patterns of secreting cells, revealing the correspondence between the inferred latent patterns and cell types, as well as the signaling pathways involved. (E) Hierarchical plot shows the inferred intercellular communication network for COMPLEMENT signaling. The left and right portions represent the autocrine and paracrine signaling to MES-like cells and other cells, respectively. The source and target are represented by solid and open circles, respectively. The edge width indicates the likelihood of communication. (F) Violin plot showing the expression of genes involved in the PDGF and COMPLEMENT signaling network among each cell type. (G) A three-dimensional plot displays the pseudotime trajectory of cell clusters. The distribution of cell subsets in 3D space. The black lines show the structure of the pseudotime trajectory. (H) Pseudotime analysis of MES-like glioma cells. (I) KEGG analysis of DEGs in MES-like/RBCK1High sub-populations. (J) DoRothEA analysis on transcription factor activity in each of the cell clusters. MES-like, mesenchymal-like states; AC-like, astrocyte-like states; NPC-like, neural-progenitor-like states; OPC-like, oligodendrocyte-progenitor-like states.

MES-like/RBCK1^{Low} tumor cells, and the residual MES-like/RBCK1^{High} population becoming resistant to immune therapy.

Furthermore, responses to immune checkpoint blockades (ICB) therapy were analyzed in glioma patients with varying levels of RBCK1 expression. Patients with higher RBCK1 expression exhibited higher TIDE scores, indicating poorer responses to immunotherapy (Fig. 6E). Moreover, we also noticed significantly higher scores of T cell exclusion programs and MDSCs in the RBCK1-high group (Fig. 6F-G). Besides, patients with abnormally high expression of RBCK1 were shown to be more prone to experiencing antitumor immune evasion, which led to a decreased response rate to ICB therapy (Fig. 6H).

3.7. Screening of potential drugs for the treating Glioma

To screen out small molecule drugs for better conquering glioma, we extracted the upregulated genes in bulk RNA-seq and scRNA-seq data sets, regarded as the targeted gene set (Fig. S9A, Supplementary Table S4). Most of the top 10 targeted genes showed significant activation in the endothelial-mesenchymal transition (EMT) signaling pathway (Fig. S9B). Gene set variation analysis (GSVA) revealed that the targeted gene set was primarily enriched in apoptosis and EMT pathways across different types of cancer (Fig. S9C).

Next, we screened 149 compounds from two drug response databases (CMAP and GDSC) to identify potential therapeutic drugs for glioma in which PD-0325901 and Selumetinib were identified as potential candidates (Figs. S9D-E). Notably, a recent study of the NCI-COG Pediatric MATCH trial confirmed the effectiveness of Selumetinib in treating low-grade glioma [48]. Additionally, PD0325901 was found to down-regulate glioma cell proliferation and migration [49]. In the RBCK1-high group, Selumetinib exhibited a lower IC50 than the low RBCK1 expression group, whereas PD-0325901 exhibited a higher IC50 (Fig. S9F), suggesting that Selumetinib may be a promising candidate drug for targeting RBCK1. The divergent effects on IC50 values between PD-0325901 and Selumetinib in the context of different expressions of RBCK1 could arise from the additional off-target effects or interactions with other cellular components. Furthermore, RBCK1 could potentially modulate the activation or expression of downstream effectors, leading to different responses to PD-0325901 and Selumetinib.

3.8. Validation of the role of RBCK1 in glioma

To verify and support bioinformation data, we performed cell loss-of-function experiments and immunocytochemistry studies. RBCK1 was found to overexpression in cancer tissues compared to para-cancerous brain tissues (Fig. 7A) and to be significantly upregulated in Grade IV glioma (Fig. 7B). Protein levels of RBCK1 were relatively high in U87MG and A172 cell lines (Fig. 7C).

Next, we knocked down RBCK1 in U118MG and A712 cells (Fig. 7D) and collected tumor-conditioned medium from transfected cells to conduct further assays on HUVECs. We found that TCM from shRBCK1 cells weakened migration capacity (Fig. 7E-F) and increased apoptosis of HUVECs (Fig. 7G-H). Furthermore, the knockdown of RBCK1 reduced the expression of the pro-angiogenic inducer, VEGFA (Fig. 7I). We then overexpressed RBCK1 and found that endogenous VEGFA expression

was subsequently increased (Fig. 7J-M). Luciferase reporter gene assay was conducted with a vector including the promoter region of VEGFA, a target gene of HIF-1α. Results showed that upregulation of RBCK1 enhanced the activities of HIF-1α luciferase reporter (Fig. 7N). To explore whether RBCK1 contributes to the effectiveness of anti-angiogenic therapy, we collected TCM from the control and RBCK1-knockdown or overexpression cells and incubated HUVECs with different TCM in the presence of Axitinib. Conditioned media of RBCK1-overexpression cells enhanced the inhibitory effects of Axitinib on HUVEC cell viability (Fig. S9G).

RBCK1 works with SHARPIN and HOIP to constitute LUBAC, which participates in the canonical NF-κB activation [9]. We found that HOIP and SHARPIN were expressed in both tumor and para-carcinoma tissues of glioma, with higher expression levels observed in the tumor tissues than in the para-carcinoma tissues (Fig. S9H). Additionally, the expression of HOIP and SHARPIN showed no significant change in RBCK1 knockdown or overexpression cells (Figs. S9I-J). Fig. S8B shows that the NF-κB transcription factor activity was upregulated in the RBCK1-high expression group. Therefore, we investigated whether RBCK1 affects the NF-κB pathway and found that IKBα phosphorylation preceded its degradation and the liberation of NF-κB subunits. Moreover, RBCK1 knockdown decreased the expression of p-IκBα and p-p65 (Fig. 7O).

3.9. Knockdown of RBCK1 suppressed glioma cell growth in vivo

As high levels of RBCK1 have been linked to unfavorable clinical outcomes in glioma patients, we investigated the effect of RBCK1 depletion on glioma cell processes. Nude mice were subcutaneously injected with RBCK1 knockdown or control tumor cells. The sh-RBCK1 group exhibited noticeably smaller tumor size, volume, and weight than the control group (Fig. 8A-C). In summary, RBCK1 was found to influence immune cell infiltrations, immunomodulatory factors, and anti-angiogenic therapy, which reshaped an inhibitory immune micro-environment. Moreover, RBCK1 participated in regulating the HIF-1α/VEGFA pathway, which could affect vascular cells and angiogenic responses. Glioma with high RBCK1 expression was observed to be weaker responsive to cancer immunotherapy but stronger to anti-angiogenic therapy (Fig. 8D).

4. Discussion

RBCK1, an E3 ubiquitin ligase, has been found to function in immune regulation and cancer progression [5,6,50]. In our pan-cancer analyses, we observed that the expression of RBCK1 was elevated in various cancers. Glioma is characterized by a unique pro-angiogenic and inflammatory microenvironment, facilitating immune escape, tumor malignant progression, and poor therapeutic efficacy. Therefore, we focused on the functions of RBCK1 in glioma to improve its treatment outcomes. Our findings suggest that RBCK1 shapes an immunosuppressive tumor microenvironment, as RBCK1 expression positively correlates with immunosuppressive factors in glioma. RBCK1 was also overexpressed, especially in the TME, indicating that anti-RBCK1 treatment may lead to fewer side effects. Therefore, anti-RBCK1

A

B

C

D

E
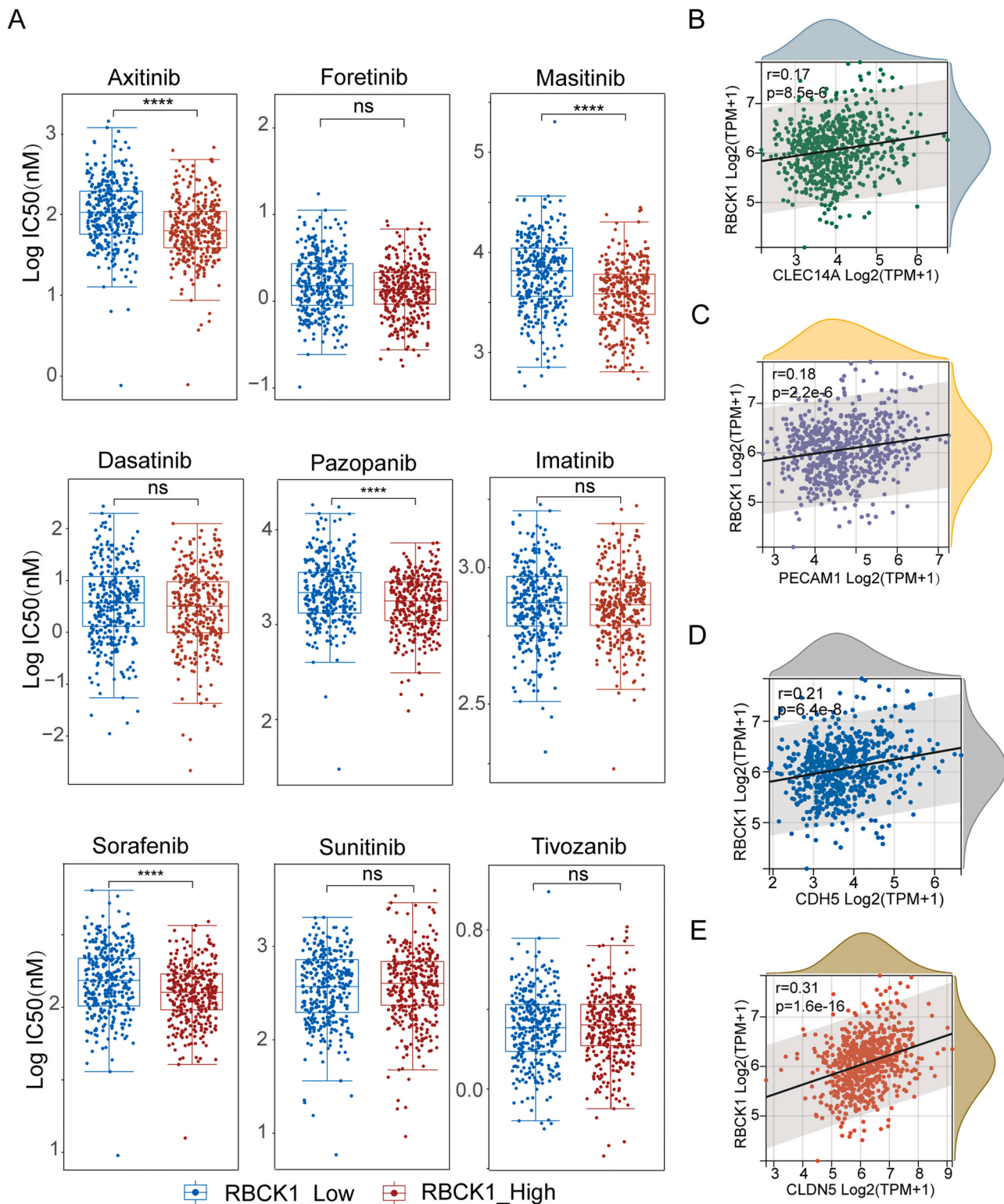
Fig. 5. Analysis of angiogenesis molecules susceptibility. (A) The IC50 for angiogenesis molecules was compared between low and high RBCK1 expression groups based on the GDSC database (Wilcoxon test). (B-E) Correlation scatter plot of RBCK1 expression and vascular endothelial marker genes in the TCGA glioma cohort (Pearson correlation analysis). ****$P < 0.0001$, ns $P > 0.05$.

immunotherapy could be a promising treatment approach for glioma.

The immune context within the TME is diverse and complex, influencing tumor epigenetics, differentiation, metastasis, and immune escape [13,51]. In the present study, upregulation of RBCK1 was found to be positively associated with immune inhibitors, including CTLA4, PD-1, and PD-L1, but inversely correlated with effector genes of NK cells

and CD8$^+$ T cells, including CD8A, CD8B, CRTAM, and NCR1 in glioma. The immune checkpoint prevents an overactive immune response, which induces immune evasion in tumors. The cancer immunity cycle, representing systemic immune recognition and elimination of cancer cells, involves the trafficking of immune cells into tumors. The expression level of RBCK1 showed a positive correlation with the trafficking of
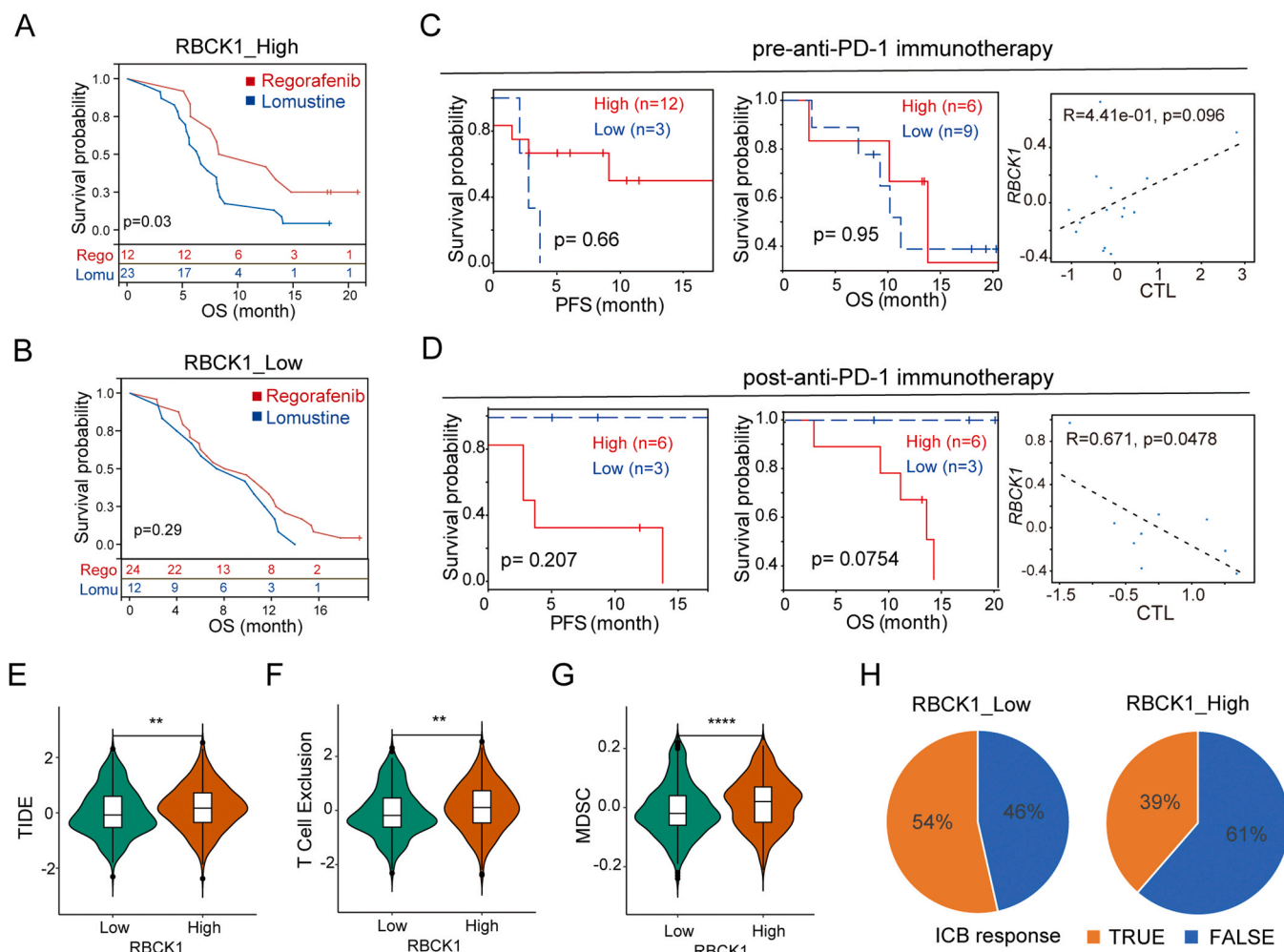
Fig. 6. Association between RBCK1 expression on antitumor efficacy in glioma and potentially applicable drugs screen. (A-B) OS curves of patients with high (A) and low (B) expression of RBCK1 who used Regorafenib or Lomustine. (C-D) RBCK1 expression with PFS, OS, and cytotoxic T lymphocytes (CTL) in glioma patients following prior to PD-1 inhibitor therapy (C) or after initiation of PD-1 inhibitor therapy (D). (E-G) TIDE scores, T cell Exclusion, and MDSC in different groups. (H) Pie chart showing the ICB response rate in different groups. ****$P < 0.0001$, **$P < 0.01$.

Th2 cells, Tregs, and MDSCs. Moreover, RBCK1 was found to play an immunosuppressive role by downregulating immunomodulator expression, such as CX3CL1/CX3CR1, leading to the downregulation of the cancer-immunity cycle activities. These results suggested that glioma with high RBCK1 expression was related to high immunosuppression of TME.

At the single-cell level, a subset of cells characterized as MES-like/RBCK1^{High} exhibited high expression of genes associated with VEGF, HIF-1, and PI3K-Akt signaling. On the other hand, MES-like/RBCK1^{Low} cells were found to potentially affect the pro-inflammatory status of macrophages and be more susceptible to T-cell-mediated killing. These findings indicate that RBCK1 may involve modifying immune cell distribution and their interactions with cancer cells, which lead to distinct prognoses for glioma patients.

A high degree of heterogeneity in gliomas poses a grand challenge to treatment decisions and prognostic assessment [16]. Although targeted inhibitors for mutant IDH have shown clinical efficacy, wild-type IDH gliomas still lack reliable therapeutic targets, resulting in a poor overall prognosis [52]. Our data indicated that RBCK1 expression was upregulated in wild-type IDH gliomas, and relatively higher copy number variations were observed in IDH-wild and MGMT unmethylated gliomas. Therefore, RBCK1 may serve as a potential molecular subtype for glioma classification. Molecular subtyping can explain the molecular heterogeneity observed in gliomas, allowing better prognosis prediction

and response to various treatment options.

Our study also revealed that an increased level of RBCK1 was linked to a decreased response rate to ICB treatment but a better response to anti-angiogenic treatment. Additionally, we screened possible targets and drugs for glioma patients with MES-like/RBCK1^{High} cell subpopulation or higher RBCK1 expression and identified two promising compounds, PD-0325901 and Selumetinib. Targeted therapies, such as blocking RBCK1 and anti-angiogenic therapy, could benefit glioma patients with high RBCK1 expression.

Despite conducting a comprehensive and systematic investigation of RBCK1 in human cancers, there were still certain limitations that should be acknowledged in this study. First, our study solely focused on bioinformatic analyses to evaluate the immunological function of RBCK1 in glioma. In our future studies, we intend to generate an orthotopic glioma mouse model to investigate the roles of RBCK1 in glioma progression and its potential immunomodulatory effects. Second, the results of screening potential drug candidates are merely based on bioinformatics analyses; a study with a larger sample size and experimental validation is required.

5. Conclusion

Our study suggests that anti-RBCK1 immunotherapy may be a promising treatment option for glioma. RBCK1 plays a role in shaping an
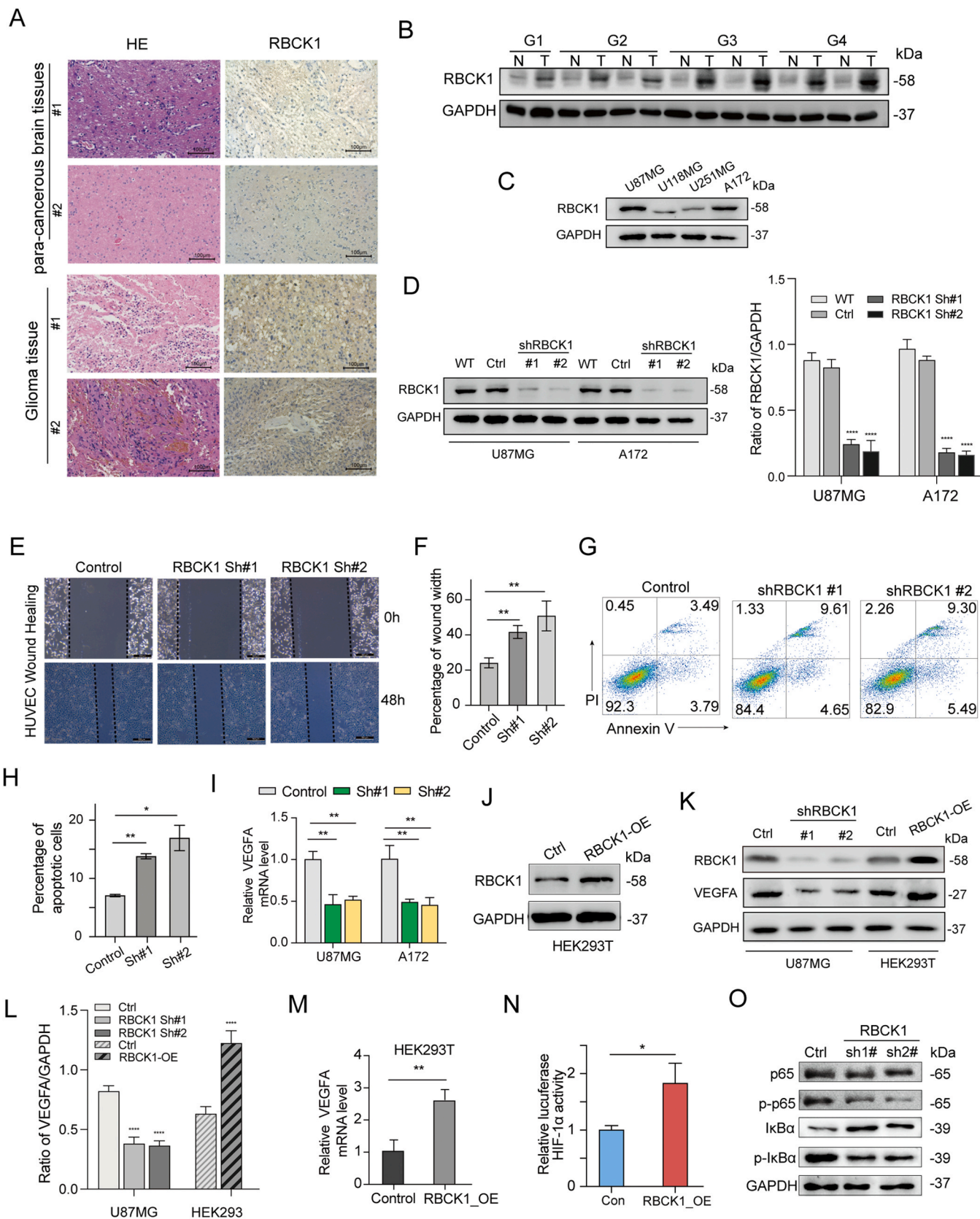
(caption on next page)

Fig. 7. RBCK1 promotes angiogenesis by increasing HIF-1α transcriptional activity and VEGFA expression. (A) The HE staining and IHC analysis of para-cancerous brain and glioma tissue. (B) RBCK1 protein expression in para-cancerous brain and glioma tissue. G1–4, grade1–4; T, tumor tissue; N, normal tissue. (C) RBCK1 expression level in four glioma cell lines. (D) Validation of the knockdown of RBCK1 in U87MG and A172 (left) and relative protein amounts were quantified via ImageJ (right). WT, wild type; Ctrl, control. (E) The typical pictures of Scratch-wound healing assay of HU-VECs incubated with TCM. (F) The bar graph indicates the quantification of the scratch test at T48h. (G-H) HUVEC apoptosis incubated with TCM was detected using flow cytometry (G) and bar-graph of associated quantification (H). (I) RBCK1 knockdown reduced mRNA expression of VEGFA. (J) Validation of RBCK1 overexpression in HEK293 cells. (K-L) VEGFA expression level in RBCK1 knockdown or overexpression cells (K) and relative protein amounts were quantified via ImageJ (L). (M) RBCK1 increased mRNA expression of VEGFA in cells. (N) Dual luciferase analysis of transcription activation activity of HIF-1α in RBCK1-overexpression cells. (O) p65, p-p65, IκBα, and p-IκBα protein expression in RBCK1 knockdown and corresponding control cells. RBCK1_OE, RBCK1 overexpression. Error bars denote mean ± SD (n = 3). ****$P < 0.0001$, **$P < 0.01$, *$P < 0.05$.
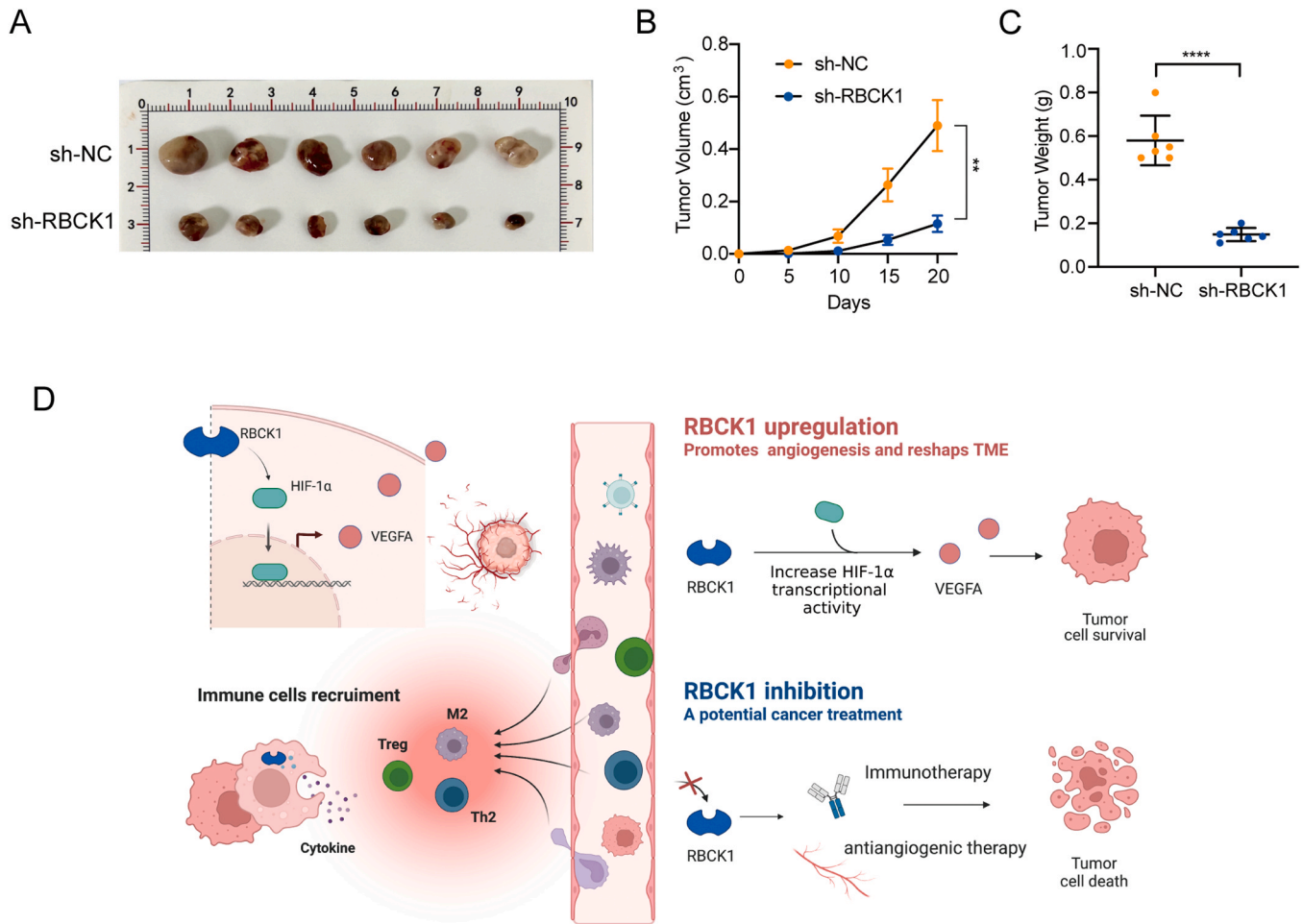
Fig. 8. Schematic diagram. (A) Tumors derived from U87 cells transfected with sh-RBCK1 or sh-NC were observed. Error bars denote mean ± SD (n = 6). (B-C) The tumor weight and volume in the sh-RBCK1 or sh-NC group were measured and calculated. (D) RBCK1 modulates the angiogenesis through the HIF-1α/VEGFA pathway and contributes to the remodeling microenvironment by regulating the infiltration of immune cells and immunomodulators. ****$P < 0.0001$, **$P < 0.01$.

immunosuppressive tumor microenvironment in glioma and can be used to predict the responsiveness of various treatments. This information can guide personalized therapy to optimize treatment efficacy.

Author contributions

J.G.: Conceptualization, Methodology, Formal analysis, Software, Writing-original draft, Writing-review & editing, Visualization. D.S. and J.Z.: Conceptualization, Methodology, Formal analysis, Investigation, Visualization. J.G, Y.C. and Y.X.: Investigation, Methodology. Z.W.: Writing-original draft, Writing-review & editing. D.Z., Y.C., Q.M. and Y. L: Investigation, Visualization. Q.Y., and T.Z.: Conceptualization, Methodology, Supervision, and Funding acquisition.

CRediT authorship contribution statement

Jing Guo: Conceptualization, Methodology, Formal analysis, Software, Writing – original draft, Visualization. **Donglin Sun:** Conceptualization, Methodology, Formal analysis, Investigation, Visualization. **Junwei Zhang:** Methodology, Formal analysis, Investigation, Visualization. **Jie Guo:** Investigation, Methodology. **Zhenpeng Wu:** Writing – original draft, Writing – review & editing. **Yongzhen Chen:** Investigation, Methodology. **Yujie Xu:** Investigation, Methodology. **Desheng Zhou:** Investigation, Visualization. **Yachao Cui:** Investigation, Visualization. **Qi Mo:** Investigation, Visualization. **Yingchang Li:** Investigation, Visualization. **Ting Zhao**: Conceptualization, Methodology, Supervision, Funding acquisition. **Qiang You**: Conceptualization, Methodology, Supervision, Funding acquisition.

Declaration of Competing Interest

The authors declare that they have no known competing financial interests or personal relationships that could have appeared to influence the work reported in this paper.

Data availability

All data used in this study are publicly available online.

Acknowledgements

None.

Supplementary Materials

Fig.mentary Fig. 1–9. Supplementary legends. Supplementary Table1: The abbreviations of various cancer types. Supplementary Table2: Domain feature of RBCK1. Supplementary Table3: The associations of the immune infiltration scores with RBCK1 expression in pancancer. Supplementary Table4: The intersection of DEGs in the TCGA and GEO (The target gene set).

Appendix A. Supporting information

Supplementary data associated with this article can be found in the online version at doi:10.1016/j.csbj.2023.10.020.

References

[1] Humphreys LM, Smith P, Chen Z, Fouad S, D'Angiolella V. The role of E3 ubiquitin ligases in the development and progression of glioblastoma. Cell Death Differ 2021;28(2):522–37.

[2] Ye P, Chi X, Cha JH, Luo S, Yang G, et al. Potential of E3 ubiquitin ligases in cancer immunity: opportunities and challenges. Cells 2021;10:12.

[3] Zhou X, Sun SC. Targeting ubiquitin signaling for cancer immunotherapy. Signal Transduct Target Ther 2021;6(1):16.

[4] Tokunaga F, Sakata S, Saeki Y, Satomi Y, Kirisako T, et al. Involvement of linear polyubiquitylation of NEMO in NF-kappaB activation. Nat Cell Biol 2009;11(2):123–32.

[5] Elton L, Carpentier I, Verhelst K, Staal J, Beyaert R. The multifaceted role of the E3 ubiquitin ligase HOIL-1: beyond linear ubiquitination. Immunol Rev 2015;266(1):208–21.

[6] Gustafsson N, Zhao C, Gustafsson JA, Dahlman-Wright K. RBCK1 drives breast cancer cell proliferation by promoting transcription of estrogen receptor alpha and cyclin B1. Cancer Res 2010;70(3):1265–74.

[7] Yu S, Dai J, Ma M, Xu T, Kong Y, et al. RBCK1 promotes p53 degradation via ubiquitination in renal cell carcinoma. Cell death Dis 2019;10(4):254.

[8] Rittinger K, Ikeda F. Linear ubiquitin chains: enzymes mechanisms and biology. Open Biol 2017;7:4.

[9] Iwai K, Fujita H, Sasaki Y. Linear ubiquitin chains: NF-κB signalling cell death and beyond. Nat Rev Mol Cell Biol 2014;15(8):503–8.

[10] Pan D, Kobayashi A, Jiang P, Ferrari de Andrade L, Tay RE, et al. A major chromatin regulator determines resistance of tumor cells to T cell-mediated killing. Science 2018;359(6377):770–5.

[11] Manguso RT, Pope HW, Zimmer MD, Brown FD, Yates KB, et al. In vivo CRISPR screening identifies Ptpn2 as a cancer immunotherapy target. Nature 2017;547(7664):413–8.

[12] Lawson KA, Sousa CM, Zhang X, Kim E, Akthar R, et al. Functional genomic landscape of cancer-intrinsic evasion of killing by T cells. Nature 2020;586(7827):120–6.

[13] Galon J, Angell HK, Bedognetti D, Marincola FM. The continuum of cancer immunosurveillance: prognostic predictive and mechanistic signatures. Immunity 2013;39(1):11–26.

[14] Binnewies M, Roberts EW, Kersten K, Chan V, Fearon DF, et al. Understanding the tumor immune microenvironment (TIME) for effective therapy. Nat Med 2018;24(5):541–50.

[15] De Palma M, Biziato D, Petrova TV. Microenvironmental regulation of tumour angiogenesis. Nat Rev Cancer 2017;17(8):457–74.

[16] Weller M, Wick W, Aldape K, Brada M, Berger M, et al. Glioma. Nat Rev Dis Prim 2015;1:15017.

[17] Xu S, Tang L, Li X, Fan F, Liu Z. Immunotherapy for glioma: current management and future application. Cancer Lett 2020;476:1–12.

[18] Smits M, van den Bent MJ. Imaging correlates of adult glioma genotypes. Radiology 2017;284(2):316–31.

[19] Galon J, Bruni D. Tumor immunology and tumor evolution: intertwined histories. Immunity 2020;52(1):55–81.

[20] Broekman ML, Maas SLN, Abels ER, Mempel TR, Krichevsky AM, et al. Multidimensional communication in the microenvirons of glioblastoma. Nat Rev Neurol 2018;14(8):482–95.

[21] Sun D, Wang J, Han Y, Dong X, Ge J, et al. TISCH: a comprehensive web resource enabling interactive single-cell transcriptome visualization of tumor microenvironment. Nucleic Acids Res 2021;49(D1):D1420–d1430.

[22] Ribas A, Wolchok JD. Cancer immunotherapy using checkpoint blockade. Science 2018;359(6382):1350–5.

[23] Greillier L, Tomasini P, Barlesi F. The clinical utility of tumor mutational burden in non-small cell lung cancer. Transl lung Cancer Res 2018;7(6):639–46.

[24] Liu Y, Sethi NS, Hinoue T, Schneider BG, Cherniack AD, et al. Comparative molecular analysis of gastrointestinal adenocarcinomas. Cancer Cell 2018;33(4):721–35. e728.

[25] Thorsson V, Gibbs DL, Brown SD, Wolf D, Bortone DS, et al. The immune landscape of cancer. Immunity 2018;48(4):812–30. e814.

[26] Yoshihara K, Shahmoradgoli M, Martínez E, Vegesna R, Kim H, et al. Inferring tumour purity and stromal and immune cell admixture from expression data. Nat Commun 2013;4:2612.

[27] Hu J, Yu A, Othmane B, Qiu D, Li H, et al. Siglec15 shapes a non-inflamed tumor microenvironment and predicts the molecular subtype in bladder cancer. Theranostics 2021;11(7):3089–108.

[28] Chen DS, Mellman I. Oncology meets immunology: the cancer-immunity cycle. Immunity 2013;39(1):1–10.

[29] Jiang P, Gu S, Pan D, Fu J, Sahu A, et al. Signatures of T cell dysfunction and exclusion predict cancer immunotherapy response. Nat Med 2018;24(10):1550–8.

[30] Jin S, Guerrero-Juarez CF, Zhang L, Chang I, Ramos R, et al. Inference and analysis of cell-cell communication using CellChat. Nat Commun 2021;12(1):1088.

[31] Garcia-Alonso L, Holland CH, Ibrahim MM, Turei D, Saez-Rodriguez J. Benchmark and integration of resources for the estimation of human transcription factor activities. Genome Res 2019;29(8):1363–75.

[32] Akbani R, Ng PK, Werner HM, Shahmoradgoli M, Zhang F, et al. A pan-cancer proteomic perspective on the cancer genome atlas. Nat Commun 2014;5:3887.

[33] Mori A, Yamashita S, Nakajima M, Hori H, Tawara A, et al. CMAP decrement as a potential diagnostic marker for ALS. Acta Neurol Scand 2016;134(1):49–53.

[34] Wang XS, Cotton TR, Trevelyan SJ, Richardson LW, Lee WT, et al. The unifying catalytic mechanism of the RING-between-RING E3 ubiquitin ligase family. Nat Commun 2023;14(1):168.

[35] Zhao P, Li L, Jiang X, Li Q. Mismatch repair deficiency/microsatellite instability-high as a predictor for anti-PD-1/PD-L1 immunotherapy efficacy. J Hematol Oncol 2019;12(1):54.

[36] Yarchoan M, Hopkins A, Jaffee EM. Tumor mutational burden and response rate to PD-1 inhibition. New Engl J Med 2017;377(25):2500–1.

[37] Sha D, Jin Z, Budczies J, Kluck K, Stenzinger A, et al. Tumor mutational burden as a predictive biomarker in solid tumors. Cancer Discov 2020;10(12):1808–25.

[38] Samstein RM, Lee CH, Shoushtari AN, Hellmann MD, Shen R, et al. Tumor mutational load predicts survival after immunotherapy across multiple cancer types. Nat Genet 2019;51(2):202–6.

[39] Topalian SL, Drake CG, Pardoll DM. Immune checkpoint blockade: a common denominator approach to cancer therapy. Cancer Cell 2015;27(4):450–61.

[40] Park MH, Lee JS, Yoon JH. High expression of CX3CL1 by tumor cells correlates with a good prognosis and increased tumor-infiltrating CD8+ T cells natural killer cells and dendritic cells in breast carcinoma. J Surg Oncol 2012;106(4):386–92.

[41] Zhang Y, Yu S, Han Y, Wang Y, Sun Y. Human leukocyte antigen-G expression and polymorphisms promote cancer development and guide cancer diagnosis/treatment. Oncol Lett 2018;15(1):699–709.

[42] Neftel C, Laffy J, Filbin MG, Hara T, Shore ME, et al. An integrative model of cellular states, plasticity, and genetics for glioblastoma. Cell 2019;178(4):835–49. e821.

[43] Hara T, Chanoch-Myers R, Mathewson ND, Myskiw C, Atta L, et al. Interactions between cancer cells and immune cells drive transitions to mesenchymal-like states in glioblastoma. Cancer Cell 2021;39(6):779–92. e711.

[44] Winkler F, Kienast Y, Fuhrmann M, Von Baumgarten L, Burgold S, et al. Imaging glioma cell invasion in vivo reveals mechanisms of dissemination and peritumoral angiogenesis. Glia 2009;57(12):1306–15.

[45] Lombardi G, De Salvo GL, Brandes AA, Eoli M, Rudà R, et al. Regorafenib compared with lomustine in patients with relapsed glioblastoma (REGOMA): a multicentre open-label randomised controlled phase 2 trial. Lancet Oncol 2019;20(1):110–9.

[46] Santangelo A, Rossato M, Lombardi G, Benfatto S, Lavezzari D, et al. A molecular signature associated with prolonged survival in glioblastoma patients treated with regorafenib. Neuro Oncol 2021;23(2):264–76.

[47] Zhao J, Chen AX, Gartrell RD, Silverman AM, Aparicio L, et al. Immune and genomic correlates of response to anti-PD-1 immunotherapy in glioblastoma. Nat Med 2019;25(3):462–9.

[48] Eckstein OS, Allen CE, Williams PM, Roy-Chowdhuri S, Patton DR, et al. Phase II study of selumetinib in children and young adults with tumors harboring activating mitogen-activated protein kinase pathway genetic alterations: arm E of the NCI-COG pediatric MATCH trial. J Clin Oncol 2022;40(20):2235–45.

[49] Shannon S, Jia D, Entersz I, Beelen P, Yu M, et al. Inhibition of glioblastoma dispersal by the MEK inhibitor PD0325901. BMC Cancer 2017;17(1):121.

[50] Taminiau A, Draime A, Tys J, Lambert B, Vandeputte J, et al. HOXA1 binds RBCK1/HOIL-1 and TRAF2 and modulates the TNF/NF-κB pathway in a transcription-independent manner. Nucleic Acids Res 2016;44(15):7331–49.

[51] Bader JE, Voss K, Rathmell JC. Targeting metabolism to improve the tumor microenvironment for cancer immunotherapy. Mol Cell 2020;78(6):1019–33.

[52] Bush NA, Butowski N. The effect of molecular diagnostics on the treatment of glioma. Curr Oncol Rep 2017;19(4):26.